J Electr Eng Technol.2016; 11(3): 781-789
http://dx.doi.org/10.5370/JEET.2016.11.3.781

ISSN(Print) 1975-0102
ISSN(Online) 2093-7423

A 3-D Steady-State Analysis of Thermal Behavior in EHV GIS Busbar

Jin Lei†, Jian-ying Zhong*, Shi-jin Wu, Zhen Wang*, Yu-jing Guo* and Xin-yan Qin****

Abstract – Busbar has been used as electric conductor within extra high voltage (EHV) gas insulated switchgear (GIS), which makes EHV GIS higher security, smaller size and lower cost. However, the main fault of GIS is overheating of busbar connection parts, circuit breaker and isolating switch contact parts, which has been already restricting development of GIS to a large extent. In this study, a coupled magneto-flow-thermal analysis is used to investigate the thermal properties of GIS busbar in steady-state. A three-dimensional (3-D) finite element model (FEM) is built to calculate multiphysics fields including electromagnetic field, flow field and thermal field in steady-state. The influences of current on the magnetic flux density, flow velocity and heat distribution has been investigated. Temperature differences of inner wall and outer wall are investigated for busbar tank and conducting rod. Considering the end effect in the busbar, temperature rise difference is compared between end sections and the middle section. In order to obtain better heat dissipation effect, diameters of conductor and tank are optimized based on temperature rise simulation results. Temperature rise tests have been done to validate the 3-D simulation model, which is observed a good correlation with the simulation results. This study provides technical support for optimized structure of the EHV GIS busbar.

Keywords: EHV GIS busbar, Steady-state, Thermal behavior, Magneto-flow-thermal, Optimized analysis

1. Introduction

The extra high voltage (EHV) gas insulated switchgear (GIS) is a new high voltage switch equipment, which has many advantages such as less occupied area, easy installation, good safety and high reliability, etc. GIS has been widely used in power plants and substations [1, 2]. The security and reliability of GIS have more and more influence on power systems. Based on the field survey and literature review, the main fault of GIS equipment is overheating of busbar connection parts, circuit breaker and isolating switch contact parts [3, 4]. The heat-emission problem will directly affect the safe operation reliability and service life of EHV GIS. Thus, a steady-state thermal analysis of the EHV GIS busbar is essential to reveal the relations among temperature, current and structural parameters. The steady-state thermal analysis in GIS busbar is a complicated multiphysics coupling problem which includes electromagnetic field, flow field and thermal field. Besides, optimization structure design of busbar make as much as possible to reduce temperature rise and improve heat dissipation effect, which has important practical significance. Therefore, the analysis of electromagnetic field, flow field, and temperature distribution of GIS busbar, to assure the safe and reliable operation of GIS has very important research significance.

In recent years, There are many previous works which have researched the EHV GIS busbar technology in many respects, such as analysis of eddy current and thermal fields [5-7], temperature distribution inside of busbar [8], [9]. Kim [10], et al. presented the coupled analysis method between the magnetic field and thermal field to calculate the temperature rise in a GIS busbar. In [11], a thermal model is developed for the busbar system to predict the temperature variation and to calculate both the steady-state and transient electrical current carrying capacity of busbar. Metwally [12] presented finite-element simulation of double circuit, three-phase GIL inside a tunnel to calculate the magnetic-flux and current densities. Reddy [13] studied the thermoelectric performance of the iTED element using fluid-thermoelectric coupled field numerical methods.

In summary, traditional research on the GIS busbar used some empirical formulas and experiments. The approach is simple and convenient, but it can't describe accurately the internal field distribution of GIS busbar. Some works combining electromagnetic field and thermal field problem do not consider the internal gas flow in the busbar. Besides, these reports about the influence of temperature rise with the other parameters of multihysics fields, such as current, magnetic flux density, flow velocity, were few. The space of both ends of busbar is narrower, which will cause contact temperature to increase in the busbar. The influence of the end effect on temperature rise is rarely reported in the busbar. The temperature difference of inner wall and outer wall is also fewer considered for tubular structures of conductor and tank. How to optimize the structure of

† Corresponding Author: Dept. of Power and Mechanical Engineering, Wuhan University, China. (jinlei@whu.edu.cn)
* Pinggao Electric Co.,Ltd., Chian. ({zhongjy, wangz, guoyujing}@pinggao.sgcc.com.cn)
** Dept. of Power and Mechanical Engineering, Wuhan University, China. ({wsj, xyqin}@whu.edu.cn)
Received: October 3, 2015; Accepted: February 1, 2016

Copyright ⓒ The Korean Institute of Electrical Engineers
This is an Open-Access article distributed under the terms of the Creative Commons Attribution Non-Commercial License (http://creativecommons.org/licenses/by-nc/3.0/) which permits unrestricted non-commercial use, distribution, and reproduction in any medium, provided the original work is properly cited.

busbar is an important topic worthy of concern based on temperature rise results.

In this paper, a coupled magneto-flow-thermal approach is used to investigate the thermal properties of GIS busbar. The skin effect and eddy current are considered in order to calculate accurately heat source. The convection coefficient is the function of structure and temperature, which is calculated by 3-D FEM. Radiation, convection and the influence of gravity are considered comprehensively in our simulation model, which makes temperature rise results more accurate. The temperature rises of conductor and tank in the compact busbars are determined by 3-D FEM simulation. Some sensors are placed in the testing busbar (ZF11C-252) and temperature rise tests are carried out. These results of simulations and tests show good agreement. This study introduces how to optimize the structure of busbar based on temperature rise results.

2. Formulation

2.1 Electromagnetic field equation

In the main conductor of a GIS, steady-state AC current flows and total current density (the sum of the source current density and eddy current density) is different with respect to its position.

$$\nabla \times \frac{1}{\mu}(\nabla \times \vec{A}) = \vec{J}_{total} = \vec{J}_s + \vec{J}_e = -\sigma \nabla \phi - j\varpi\sigma \vec{A} \qquad (1)$$

where J_{total} is the total current, J_s the source current density, J_e the eddy current density, σ is the electric conductivity, ϕ is magnetic flux, $\vec{A}$ is vector magnetic potential. Using Maxwell's equation in which the magnetic vector potential and the electric scalar potential are introduced, the eddy current field equations can be written as [14]

$$\nabla \times \nu \nabla \times \vec{A} - \nabla \nu \nabla \cdot \vec{A} = \vec{J}_s \quad in\ \Omega_1 \qquad (2)$$

$$\left.\begin{aligned} &\nabla \times \nu \nabla \times \vec{A} - \nabla \nu \nabla \cdot \vec{A} + \sigma \nabla \vec{\phi} + j\varpi\sigma \vec{A} = 0 \\ &\nabla \cdot (\sigma \nabla \vec{\phi} - j\varpi\sigma \vec{A}) = 0 \end{aligned}\right\} in\ \Omega_2 \qquad (3)$$

where Ω_1 is the area with source current, Ω_2 is the other area without source current.

2.2 Power loss

The power loss is generated in the main conductor and enclosure tank. Using the current distribution from Eq. (1), the power loss density is calculated by:

$$Q = \frac{1}{\sigma}\left|J_{total}{}^2\right| = \frac{1}{\sigma}\left|\sigma E\right|^2 = \sigma\left|\Delta V\right|^2 \qquad (4)$$

where σ is the electric conductivity and a function of temperature.

2.3 Flow field equation

The governing equations of nonisothermal flow can be written for the flow phase Ω_{flow}, i.e. SF_6 gas and air as follows:

$$\begin{aligned} &\rho(u \cdot \nabla)u = \nabla \cdot \left[-PI + \mu(\nabla u + (\nabla u)^{\mathrm{T}}) - \frac{2}{3}\mu(\nabla \cdot u)I\right] + F \\ &\nabla \cdot (\rho u) = 0 \\ &\rho C_p u \cdot \nabla T = \nabla \cdot (k \nabla T) + Q + Q_{vh} + W_p \end{aligned} \qquad (5)$$

where P denotes gas pressure (P_a); I identity matrix; F is volume force (N).

2.4 Thermal field equation

As for the conducting rod, when heat balance achieves steady, its loss (P_c) passes to the tank in two ways: convection (Q_{cc}) and radiation (Q_{cr}). They meet the balance equation: $P_c = Q_{cc} + Q_{cr}$. As for busbar tank, total losses is the heat loss (P_K) itself and the heat from conducting rod (P_t). This heat by radiation (Q_{tr}) and natural convection (Q_{tc}) send to the surrounding environment. The second balance equation can be derived as follows:

$$P_t + P_k = Q_{tc} + Q_{tr}.$$

The corresponding temperature rises can be computed using magneto-thermal-flow 3-D FEM to solve the following thermal equations:

$$\begin{aligned} &\Omega : \nabla \cdot \lambda \nabla T = Q_v \\ &\Gamma_1 : T = T_C \\ &\Gamma_2 : \lambda \frac{\partial T}{\partial n} = k_T (T_\infty - T) \end{aligned} \qquad (6)$$

where Ω is the solved area, Γ is the boundary, λ is the coefficient of heat conductivity, Q_v is the heat power per unit volume, k_T is the heat transfer coefficient. T is the temperature, T_∞ is the ambient temperature.

Conductor radiation heat exchange between the outer wall of conductor and the wall of tank:

$$Q_{cr} = \frac{\sigma A_{co}(T_c^4 - T_t^4)}{\frac{1}{\varepsilon_c} + \frac{A_{co}}{A_{ti}}(\frac{1}{\varepsilon_t} - 1)} \qquad (7)$$

where $\sigma = 5.67 \times 10^{-8}$ is Stefan-Boltzmann constant; ε is conductor surface emissivity; A_{co} and A_{ti} are the surface of the external surface of the conductor and the internal surface of busbar tank, respectively.

The radiation heat exchange between busbar tank's wall

and outer space is given by the expression

$$Q_{tr} = \varepsilon_t \sigma A_{to} (T_t^4 - T_\infty^4) \quad (8)$$

where A_{to} is length of the shell surface area for the unit.

The heat transfer coefficient is an empirical parameter that incorporates the heat transfer relationship and the nature of the air flow pattern near the surface, the air properties and the geometry of the outside surfaces. Besides, the Nusselt number is a nondimensional heat transmission coefficient defined by the following equation:

$$Nu = \frac{h_c L}{\alpha \cdot \Delta T} \quad (9)$$

where h_c is the surface convective heat transfer coefficient, L is the characteristic length, α is conductivity coefficient of fluid, ΔT is temperature difference of the wall and the fluid. Equation (9) gives a measure of the heat energy transferred per unit time and per unit area to the outside busbar surfaces.

The boundary conditions are set as follows: the material surface emissivity on the outer surface of conductor is 0.7. The surface emissivity on the outer wall of tank is 0.7. Tc and Tt was calculated as the algorithm in the process of iteration; the outer space environment temperature is set to 25°C.

3. Geometry and Modelling

3.1 The structure of GIS busbar

The busbar is the key part of EHV GIS equipment, which is used as electric conductor to reduce overall size and cost. The busbar in general involves three external components which are shield housing, busbar tank and epoxy insulator and three internal components which are conducting rod, spring contact and V-groove as shown in Fig. 1. Conducting rod is installed in busbar tank and supported by epoxy insulator. There is SF_6 gas insulation medium at a certain pressure between rod and shell. The specific design of spring contact using plug-in configurations is applied in present products, which can provide ample angular deflection for easier assembling or dismantling operations. The spring contact with canted coil is mounted in the shield housing that has four V-grooves, the insertion of a conducting rod is ensuring the electrical continuity. Connecting conductors are made of aluminum alloy with high-grade, silver-plated contacts on its surfaces. Their sliding capability allows thermal expansion without transmitting mechanical stress to insulators.

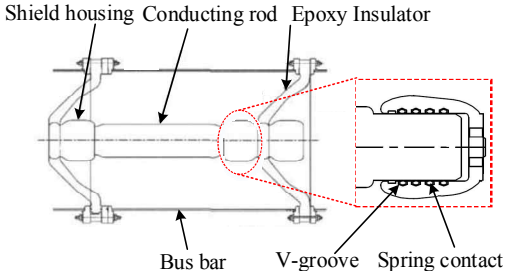

Fig. 1. The structure of EHV GIS busbar assembly

3.2 3-D Simulation model

In recent years, in order to overcome the limitations of traditional methods, some researchers tend to adopt FEM to solve the power loss, eddy current, temperature rise, *etc.* [4, 6, 7]. In the study, a coupled magneto-thermal-flow 3-D FEM is used to investigate the thermal properties of EHV GIS busbar in steady-state. A simplified 3-D simulation model is shown as in Fig. 2.

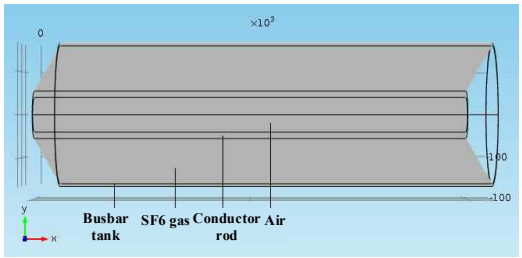

Fig. 2. The 3-D FEM simulation model of EHV GIS busbar

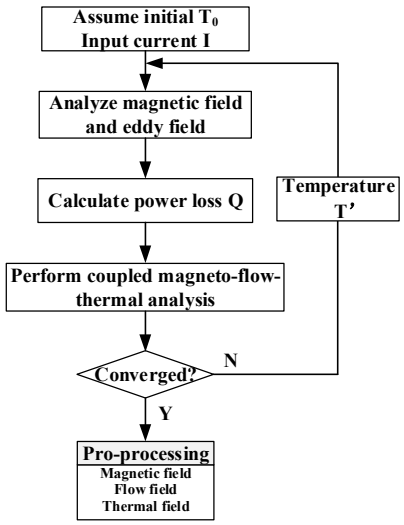

Fig. 3. The schematic procedure of the 3D coupled magneto-thermal-flow analysis

Table 1. Dimension of EHV GIS busbar model

Component	Material	Parameter	Value
Conducting rod	Aluminum 6063	Inner diameter (mm)	80
		Outer diameter(mm)	110
Busbar tank	Aluminum 5052	Inner diameter (mm)	320
		Outer diameter (mm)	332

Table 2. Parameters of air and SF_6 gas

Spec.	Pressure (MPa)	Dynamic viscosity (m^2/s)	Thermal conductivity (W/m°C)
Air	0.1	19.6e-06	0.0286
SF_6	0.4	1.3e-06	0.0153

The schematic procedure of the coupled magneto-thermal-flow analysis by 3-D finite element method is shown in Fig. 3. The use of COMSOL multiphysics is to simulate and optimize the GIS busbar in this study.

These primary dimensions of the EHV GIS busbar are given in Table 1. The required properties for SF_6 gas and air are listed in Table 2.

4. Results and tests

4.1 Electromagnetic field

It is well known that conductor with large current will induce magnetic field. In the meantime, power frequency current will also induce eddy current on surface of metal, which transformed into a lot of heat. Therefore, the calculation of the magnetic field is the first step to obtain temperature rise.

The magnetic flux density can be calculated by loading 4.0kA 50Hz current as shown in Fig. 4, which shows that magnetic flux density gradually increases from inner to outer in the conducting rod. It reaches the peak on the outer edge. On the contrary, magnetic flux density gradually decreases from inner wall to outer wall of busbar tank, which decays smaller in the busbar tank. The peak of magnetic flux density is about 0.0146 T on the outer edge of conducting rod.

By means of a 2D model it is possible to plot the magnetic flux density profile along horizontal line. The horizontal line (DD') is represented in Fig. 4 and the plot results are presented in Fig. 5. From the analysis of Fig. 5 it is possible to show that the magnetic flux density along the horizontal line is symmetrical. The segments BC and B'C'

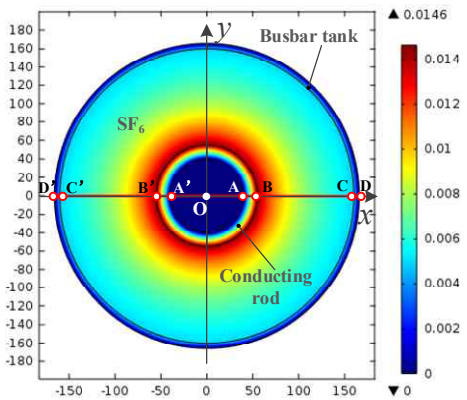

Fig. 4. Magnetic flux density in busbar at 4.0kA current

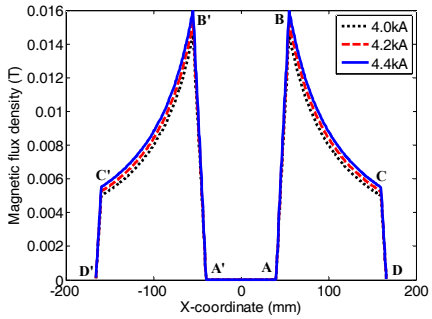

Fig. 5. The distribution of magnetic flux density at different currents

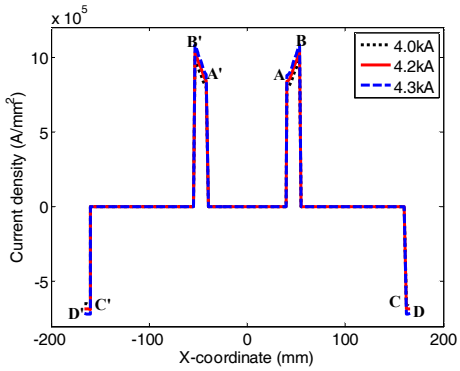

Fig. 6. The distribution of current density with different currents in busbar

present apparent nonlinearity, and the magnetic flux density decrease significantly from 0.016T to 0.005T. Because of attribute of SF_6 gas medium, magnetic field intensity decays nonlinearly in SF_6 gas. These segments AB, A'B', CD and C'D' present linearity as a whole. Magnetic flux density increase slightly with the increasing currents in the busbar as seen in Fig. 5.

Due to eddy current and skin effect, the current density in conducting rod decreases from the inner surface of 1091905 A/m^2 to the outer wall of 875529 A/m^2 in Fig. 6. The current density along the horizontal line is also symmetrical. The current on the busbar tank induced current is the opposite direction to that of the source current, so it is negative. The current density of inner wall is bigger than outer wall's in the busbar tank. The current density in the conductor increases with increasing currents presented in segments AB, A'B', CD and C'D'.

4.2 Flow field

Because of the uneven heating and gravity, the heated SF_6 gas will flow along a certain path. The flow of SF_6 gas can change temperature distribution in the busbar. Therefore, the influence of flow field is critical for temperature distribution. The structure of busbar is symmetry in 2-D cross section, the cooling paths of gas inside the busbar tank are same, and so the distribution of gas flow is symmetrical along horizontal direction. The

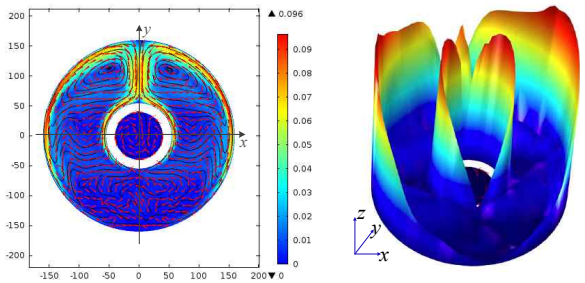

Fig. 7. Flow velocity distribution of GIS busbar model: (a) 2-D Cross section view; (b) 3-D display

distribution of flow velocity of the GIS busbar model is shown in Fig. 7 (a). Because of the influence of gas flow by gravity, the flow velocity of the top is bigger than the bottom in the busbar. The peak velocity in the SF_6 gas domain reaches 0.0932 m/s on the top of conducting rod. There are two vortexes at both sides of the busbar as seen in Fig. 7 (a).

The internal isotherms in the busbar are not concentric circles, of which temperature declines monotonously along radius direction, but rather S-shape distribution as seen in Fig. 7(b). Besides, along the direction of the radius in the annular space, it appears that flow velocity of SF_6 gas increases farther away from hot surface. When conducting rod is loaded rated current, lots of heat will be generated from conducting rod. SF_6 gas around conducting rod is heated, which leads to decrease density of SF_6 gas. When heated SF_6 gas flows upward and its temperature gradually reduces, SF_6 gas will develop backflow along both sides of inner wall of busbar. It is clearly seen that gas flow path is S-shape in Fig. 7(b).

Fig. 7 only shows gas flow state in 2-D middle section of busbar, but GIS busbar is not the normal cylindrical. Its left side is convex and its right side is concave as shown in Fig. 8. In order to reveal the influence of end effect, six cross sections are chose at both ends as shown in Fig. 8. These gas flow distributions are summarized in Fig. 9.

Compared with Fig. 7, gas flow path of sections 1, 2, 4 and 5 are not complete S-path on account of end effect as seen in Fig. 9. There are obvious differences between sections 1-3 on the left and sections 4-6 on the right. The peak velocity appears around conducting rod in sections 1-3 and flow velocity is relatively large at both sides of inner wall of busbar tank in sections 4-6. This reason is that natural convection spaces of both sides in the annulus between horizontal concentric cylinders are different.

4.3 Thermal field

Based on coupled magneto-flow-thermal analysis, the 3-D FEM is employed for obtaining the distribution of velocity and temperature. Figure 10 shows temperature distribution in the 2-D middle section. Due to the influence of convection, radiation, and conduction, the distribution of

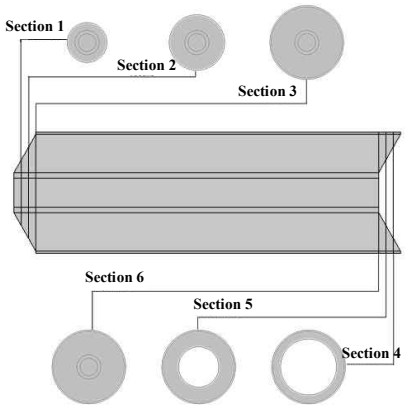

Fig. 8. Schematic of position of six cross sections

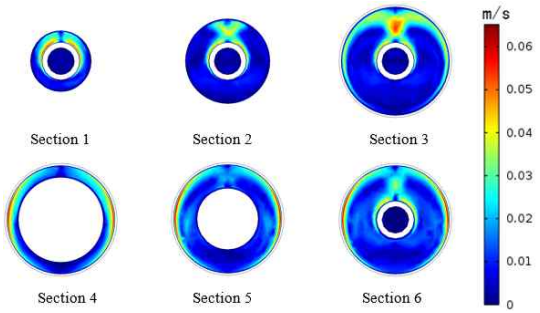

Fig. 9. Velocity distributions of the six cross sections

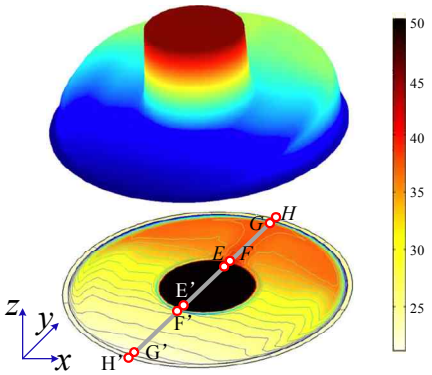

Fig. 10. Temperature distribution of the midsection and reference line HH'

temperature field is also symmetrical along x direction. In the SF_6 annulus space, temperature rise of the upper half is higher than the lower half's along y-axis direction. The peak temperature rise appears in conducting rod, and it is about 50°C.

To reveal clearly temperature distribution in the busbar, it is possible to plot the temperature rise profile along reference line HH'. The reference line (HH') is represented in Fig. 10 and the plot results are shown in Fig. 11. The three segments GH, G'H' and F'F are basically a horizontal line, which shows temperature variation is small in the rod and tank. The materials of conducting rod and busbar tank are aluminum alloy and wall thickness is 30mm. Temperature variation is bigger for segments F'G' and FG,

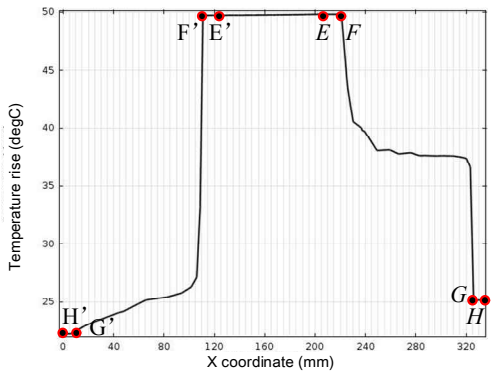

Fig. 11. Temperature rise plot along reference line HH'

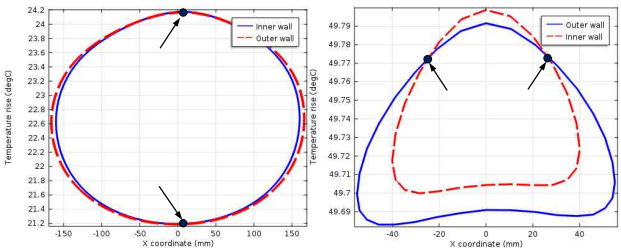

(a) (b)

Fig. 12. Temperature rises of inner wall and outer wall: (a) Busbar tank; (b) Conducting rod

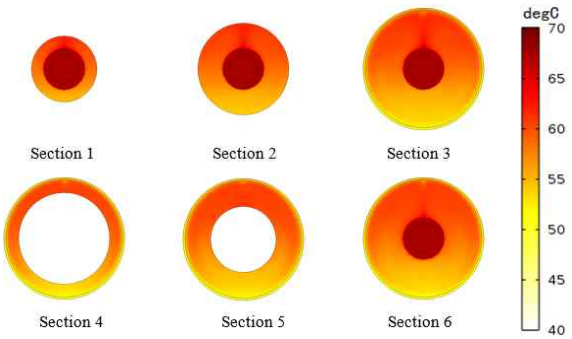

Fig. 13. Temperature distributions of the six cross sections

which causes by convection of SF_6 gas in the annulus space.

Fig. 12 shows temperature differences of inner wall and outer wall for conducting rod and busbar tank. Temperature variations is about 3°C between the bottom and top of the busbar tank in Fig. 12 (a). Temperature values of inner wall and outer wall are same at the top and the bottom. Temperature difference is bigger at both sides. From Fig. 12 (b), it can be seen that temperature difference is less than 1°C. The isothermal points appear on both sides of the top half of conducting rod.

To analyze the influence of end effect on temperature rise, temperature distributions of sections 1-6 are shown as in Fig. 13. There are same temperature distributions of conducting rod among sections 1-6. Temperature rise of busbar tank is highest in section 1, temperature of busbar tank in section 2 is the second highest. The rest of sections

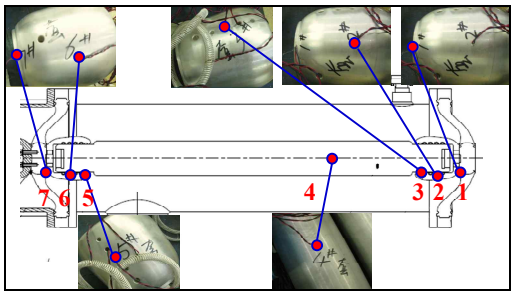

(a)

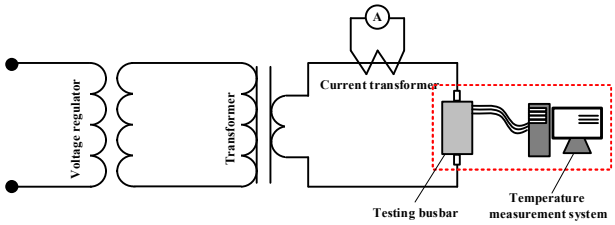

(b)

Fig. 14. Schematic diagram of temperature rise tests. (a) The positions of the seven sensors; (b) Testing main circuit

in busbar tank have about the same temperature rise. This reason is that natural convection spaces of sections 1-2 in the annulus are narrow compared with the rest of sections. Heat of conducting rod is passed to the busbar by natural convection and radiation.

4.4 Test validation

To validate the simulation model and the proposed method, some tests have been made. The diagram used for experimental tests is shown in Fig. 14. Seven temperature sensors which choose T-type thermocouples are placed in the busbar in Fig. 14 (a). To obtain more thermal behavior in contact parts, Sensors 1-3 and 5-7 are symmetrically placed in both ends of the busbar. The type of the testing busbar is the ZF11C-252. The testing busbar attached sensors is connected to the main circuit which mainly includes voltage regulator, current transformer, transformer, etc. as seen in Fig. 14 (b). Temperature rise results are recorded with a 252kv 4kA 4.4 kA by temperature measurement system after eight hours. The pressure of SF_6 gas is 0.43Mpa, and current temperature is 25 degrees, wind speed is less than 0.5 m/s in the experimental environment.

Experimental results of seven test points are plotted in Fig. 15. When current is loaded from 4.0 kA to 4.4 kA, temperatures of all test points in the busbar increase about 10°C. Temperature of test points 3 and 5 is higher than the rest positions, which is temperature of contact point between conducting rod and spring contact in the V-groove. Because of difference of heat transfer conditions of both ends, the temperature on the left is lower than on the right (test points 1 and 7). Heat transfer mode is SF_6 convection,

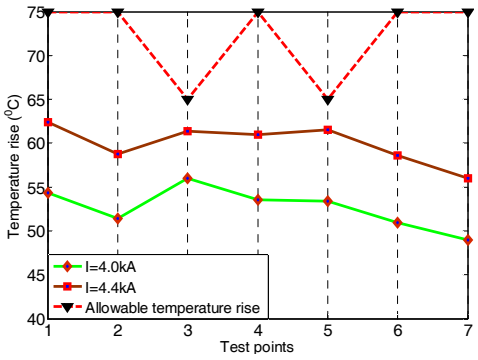

Fig. 15. Temperature rise of experimental results

Table 3. Simulation results and test results

Temperature (°C)	Maximum temperature rise		Relative
	Simulated (*I*=4kA)	Measured (*I*=4kA)	error (%)
Conducting bar	50	50.97	1.9
Busbar tank	21	20.88	0.57

radiation and conduction on the left, which compares with natural convection and radiation to surroundings on the right. Therefore, heat transfer condition on the left is better than on the right. It is noticed that temperature of contact point (test points 3 or 5) is highest in the busbar while allowable temperature rise on the point is lowest of 65°C. Therefore, the contact temperature control is critical for the reliability and safety of GIS.

Table 3 shows the comparison of temperature rise between measured and simulated results. The temperature distribution in the busbar by the proposed method shows good agreement with the experimental results within 5% of the maximum relative error.

5. Discussion

Structure parameters of GIS busbar directly affect the thermal behavior during rated working. Optimal design of structural parameter is very necessary for reliability and safety of the GIS. There are main two structural parameters for conducting rod and busbar tank, i.e. inner diameter and outer diameter. In order to consider which parameter's influence is bigger and which parameter combination is more optimized, single parameter will be changed in each thermal analysis. Temperature rise can be allow the clear identification of cause and effect because only single parameter is changed at a time, so that the effect of that single parameter can be determined.

5.1 Effects of conducting Rod's diameters

When GIS busbar is loaded rated current, heat is generated from heat loss of the conducting rod. In order to reveal the effects of changes of conducting rod's diameters,

Table 4. The diameter combinations of conducting rod

No.	Inner diameter (mm)	Outer diameter (mm)	Cross area (m^2)
A1	60	110	0.00667
B1	64	110	0.00628
C1	68	110	0.00587
D1	72	110	0.00543
E1	76	110	0.00497
F1	80	110	0.00448
G1	80	112.8	0.00497
H1	80	115.4	0.00543
I1	80	117.8	0.00587
J1	80	120	0.00628
K1	80	122.06	0.00667

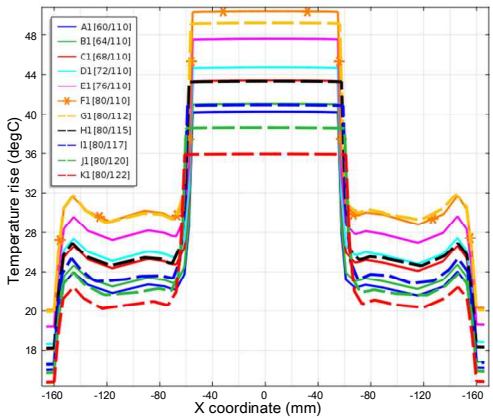

Fig. 16. Temperature rise variation with the changes of diameters along x-axis

these schemes are chosen to calculate temperature rise as seen in Table 4. From Table 4, inner diameter changes from 60mm to 80mm and outer diameter changes from 110mm to 122mm, which makes up 11 combinations. At this time, the inner diameter and outer diameter of tank are fixed to 320mm and 332mmm, respectively. Diameter change will result in change of cross area. For comparison, cross areas of five groups are set to equal (A1-K1, B1-J1, C1-I1, D1-H1, E1-G1).

For fixed the diameter of busbar tank, the eleven schemes are calculated temperature distribution in the busbar along x-axis at the same current as shown in Fig. 16. When outer diameter of conducting rod is fixed 110mm, temperature rise will reduce with the decrease of inner diameter. Besides, when inner diameter is fixed to 80mm, temperature rise will also reduce with the increase of outer diameter. Compared to the same cross area five groups, the change of conducting rod's outer diameter affect temperature rise more markedly.

5.2 Effects of busbar tank's diameters

The diameters of the busbar tank directly influence the effect of SF_6 convection and heat radiation. To reveal the effects of changes of busbar tank's diameters, design

Table 5. The diameter combinations of busbar tank

No.	Inner diameter (mm)	Outer diameter (mm)	Cross area (m^2)
A2	300.00	332.00	0.01588
B2	304.00	332.00	0.01399
C2	308.00	332.00	0.01206
D2	312.00	332.00	0.01012
E2	316.00	332.00	0.00814
F2	320.00	332.00	0.00614
G2	320.00	335.80	0.00814
H2	320.00	339.52	0.01012
I2	320.00	343.16	0.01206
J2	320.00	346.72	0.01399
K2	320.00	350.18	0.01588

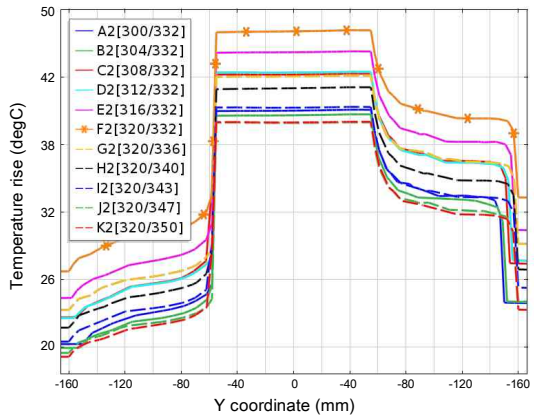

Fig. 17. Temperature rise variation with the changes of diameters of tank

schemes are listed to calculate temperature distribution in Table 5. Inner diameter changes from 300mm to 320mm and outer diameter changes from 332mm to 350mm. The inner diameter and outer diameter of conductor are fixed to 80mm and 110mmm. Similarly, cross areas of five groups are set to equal (A2-K2, B2-J2, C2-I2, D2-H2, E2-G2).

Fig. 17 shows that these schemes are calculated temperature rise along y-axis loaded current. When outer diameter of conducting rod is fixed to 332mm, temperature rise will rise with the increase of inner diameter. Besides, when inner diameter is fixed to 320mm, temperature rise will also reduce with the increase of outer diameter. Compared to the same cross area five groups, the change of busbar tank's outer diameter affect temperature rise more apparently.

From the above simulations, it is not hard to see that the increase of cross-sectional area of rod and tank will reduce temperature rise within a safer range. But the cross-sectional area will increase the economic cost and influence upon the sizes of the other components. Therefore, the optimal scheme is to consider not only heat consumption but also economic cost. The outer diameters of rod and tank are higher sensitive parameters, which can change the parameters to control effectively temperature rise.

6. Conclusions

In the study, a large number of simulations reveal thermal behavior of conducting rod/busbar tank in steady-state. The coupled magneto-flow-thermal equations are derived, which helps us to comprehend the relations of parameters of multiphysics field in theory. To calculate accurately the heat source, the skin effect and eddy current of AC current are considered in the 3-D simulation model. Considering radiation, convection and gas gravity, multiphysics field will be obtained more accurate computational solutions. The magnetic flux density, flow velocity and temperature rise of the EHV GIS busbar model are calculated by 3-D FEM analysis. Flow velocity is not uniform on a circumference but "S" type distribution. In the arbitrary 2-D cross section of the middle of busbar, the temperature distribution shows that left and right sides is symmetrical, and upper section is higher than bottom half. Because of the narrow space of both ends of busbar, convection and heat dissipation are inadequate with respect to the middle segment. Temperature rise of both ends is higher than the middle by 3-D simulation. Besides, temperature differences of inner wall and outer wall are investigated for busbar tank and conducting rod, which helps to guide the layouts of temperature sensors.

A further optimum structural design has been carried out by considering the different diameters combinations, which reveals the relation between structural parameters and temperature rise. Temperature rise tests have been achieved to validate the simulation model and the proposed method. The temperature distribution in EHV GIS busbar by the proposed method shows good agreement with the experimental results, which shows that the proposed method is effective and feasible.

Acknowledgements

This work was supported by the China Postdoctoral Science Foundation Funded (2013M542055).

References

[1] Th. A. Paul, M. Porus, B. Galletti, A. Kramer, "SF_6 concentration sensor for gas-insulated electrical switchgear Original," *Sensors and Actuators A: Physical*, vol. 206, pp. 51-56, 2014.

[2] K. Umar, "Electric Field Characteristics Inside Three-phase Gas Insulated Switchgear in the Presence of Foreign Metallic Particle Original," *Procedia Technology*, vol. 11, pp. 1195-1201, 2013.

[3] N. Raj, S. Sushant, "Study of gas insulated substation and its comparison with air insulated substation," *Electrical Power and Energy Systems*, vol.55, pp.481-485, 2014.

[4] J. K. Kim, J. Y. Lee, S. B. Wee, *et al*., "Hahn S C. A Novel Coupled Magneto-Thermal-Flow Analysis for Temperature Rise Prediction of Power Apparatus," *Electrical Machines and Systems*, vol. 43, pp. 585-588, 2008.
[5] J. Paulke, H. Weichert, P. Steinhaeuser, "Thermal simulation of switchgear," *IEEE Transactions on Components and Packaging Technologies*, vol. 25, no. 3, pp. 6-11, 2002.
[6] S. L. Ho, Y. Li, X. Lin, *et al*., "Calculations of Eddy Current, Fluid, and Thermal Fields in an Air Insulated Bus Duct System," *IEEE Transactions on Magnetics*, vol. 43, no. 4, pp. 1433-1436, 2007.
[7] S. L. Ho, Y. Li, X. Lin, H. C. Wong, *et al*., "A 3-D Study of Eddy Current Field and Temperature Rises in a Compact Bus Duct System," *IEEE Transactions on Magnetics*, vol. 42, no. 4, pp. 987-990, 2006.
[8] A. B. Wu, D. G. Chen, "Evaluation of Thermal Performance for Air-Insulated Busbar Trunking System by Coupled Magneto-Fluid-Thermal Fields," *Power System Technology*, vol. 4, pp. 13-17, 2002.
[9] C. C. Hwang, "Analysis of Electromagnetic and Termal Fields for a Bus Duct System," *Electric Power System Research*, vol. 45, no. 1, pp. 39-45, 1998.
[10] H. K. Kim, Y. H. Oh and S. H. Lee, "Calculation of temperature rise in gas insulated busbar by coupled magneto-thermal-fluid analysis," *Journal of electrical engineering technology*, vol. 4, no. 4, pp. 510-514, 2009.
[11] S. Thirumurugaveerakumar, M. Sakthivel, and S. Valarmathi, "Experimental and Analytical Study on the Bus Duct System for the Prediction of Temperature Variations Due To the Fluctuation of Load," *Journal of electrical engineering technology*, vol. 9, no. 6, pp. 2036-2041, 2014.
[12] I. A. Metwally, "Thermal and magnetic analyses of gas-insulated lines," *Electric Power Systems Research*, vol.79, pp.1255-1262, 2009.
[13] B. V. K. Reddy, M. Barry, J. Li, *et al*., "Three-dimensional multiphysics coupled field analysis of an integrated thermoelected device," *Numerical Heat Transfer, Part A*, vol.62, pp.933-947, 2012.
[14] M. N. Ozisik, "Heat Transfer A Basic Approach," *McGraw-Hill Publishing Company*, 1990.

Jin Lei received the Ph.D. degree in Mechanical Science and Engineering from Huazhong University of Science and Technology, Wuhan, China, in 2010. He joined the faculty of the Department of Power and Mechanical, Wuhan University in 2010. His research interests include multiphysics fields modelling and simulation, finite element analysis, power system simulation and structural optimization.

Jianying Zhong received the Ph.D. degree in Electricity & Automatization from Xian Jiaotong University, China, in 1999. She is currently the vice president of engineering in the Henan Ping Zhi high voltage switch Co., Ltd., China. Her research interests include power transmission switch equipment.

Shijin Wu is a professor and doctoral tutor in Department of Power and Mechanical in Wuhan University, Wuhan, China. He is currently the director of graduate school of Wuhan University. His research interests include electric power construction, and electrical hydraulic system.

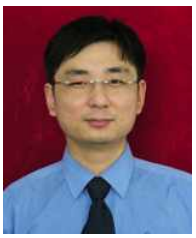

Zhen Wang received the B.S. degree in Electrical Engineering from Nanjing University of Science & Technology, China, in 1999. He is currently a senior engineer in the Henan Ping Zhi high voltage switch Co., Ltd., China. His research interests include structural design and optimization of GIS.

Yujing Guo received Ph.D. degree in mechanical electronic engineering from Chongqing University in Chong-qing, China, in 2009. He is currently a director of technology center in the Pinggao Electric Company Limited, China. His research interests include key technology and product development of high voltage switch device.

Xinyan Qin received B.S. and M.S. degree in information technology from Central China Normal University in Wuhan, Wuhan, China, in 1999 and 2004, respectively. Currently she is a Ph.D. candidate in Department of Power and Mechanical in Wuhan University, Wuhan, China. Her research interests are multi-sensor data fusion technique, power robotic and power system modelling.